

# QUANTUM MECHANICAL TREATMENT OF ION COLLISIONS WITH MANY-ELECTRON ATOMS

H.J. LÜDDE

*Institut für Theoretische Physik, Johann Wolfgang Goethe Universität, Robert Mayer Strasse 8,  
D-60054 Frankfurt, Germany*

*E-mail: luedde@th.physik.uni-frankfurt.de*

T. KIRCHNER AND M. HORBATSCH

*Department of Physics and Astronomy, York University, Toronto, Ontario, Canada M3J 1P3*

Based on the concepts of time-dependent density functional theory we present calculations for multiple electron processes in ion-atom collisions. The gist of this article is to reveal the different facets of the electronic interaction associated with different levels of approximation of the inter-electronic potential. In particular, we discuss exchange effects, Pauli blocking and response effects in collisions between protons, helium and carbon ions and rare gas atoms.

## 1 Introduction

With the advent of COLTRIMS technology atomic collisions can now be analyzed with an accuracy that allows detailed insight into the mechanisms which control many-electron systems far from equilibrium <sup>1</sup>. The interpretation of the increasingly complex experiments, however, requires a deeper theoretical understanding of the role of the electronic interaction in a dynamical quantum system.

Although the hamiltonian of a many-electron system is well known, the dynamics of the underlying time-dependent many-body quantum problem cannot be resolved exactly and remain largely unexplored. So far the only a priori non-perturbative approach to the description of collision problems involving more than two active electrons is restricted to the level of the time-dependent Hartree-Fock approximation <sup>2</sup> or approximations thereof. The aim of this project is to investigate effects associated with the electronic interaction systematically by controlled approximations of the system's many-body hamiltonian.

## 2 Theory

The non-perturbative description of collisions between ions and atoms or more complex systems like molecules, clusters or surfaces relies on a semiclassical picture: the motion of the nuclei can be adequately approximated by classical trajectories leading to a time-dependent quantum-dynamic description of the many-electron problem <sup>3</sup>. For impact energies ranging from 100 eV/amu to 10 MeV/amu and light nuclei the time-dependent Schrödinger equation (TDSE) for the electronic motion

$$(\hat{H}(t) - i\partial_t)|\Psi(t)\rangle = 0, \quad |\Psi(t_0)\rangle = |\Psi_0\rangle \quad (1)$$

is the common starting point with the many-electron hamiltonian (in atomic units)

$$\hat{H}(t) = \hat{T} + \hat{V}_{ee} + \hat{V}_{\text{ext}}(t) \quad (2)$$

$$= \sum_{i=1}^N \left( -\frac{1}{2} \Delta_i \right) + \sum_{i < j}^N \frac{1}{|\mathbf{r}_i - \mathbf{r}_j|} + \sum_{i=1}^N \left( \frac{-Q_T}{r_i} + \frac{-Q_P}{|\mathbf{r}_i - \mathbf{R}(t)|} \right). \quad (3)$$

The segmentation (2) of the hamiltonian already indicates the complexity of the problem: the universal part  $\hat{V}_{ee}$  includes the two-body interactions between the electrons (a priori time-independent) while the external potential introduces the geometry of the particular quantum system (equation (3) shows the explicit expression for ion-atom collisions). The latter is explicitly time-dependent through the classical motion of the projectile denoted by  $\mathbf{R}(t)$ . One thus has to cope with the collision problem on three levels: (i) the approximation of the time-dependent many-particle problem, (ii) the numerical solution of the resulting equations, and eventually (iii) the calculation of a large variety of many-electron observables from the final wave function  $\Psi(t \rightarrow \infty)$ .

### 2.1 The many-electron problem

If one is investigating a quantum system with many active electrons, time-dependent density functional theory (TDDFT) provides an elegant formulation of the many-particle problem in terms of effective single-particle equations<sup>4</sup>. The basic TDDFT theorem states that many-particle observables are unique functionals of the exact single-particle density

$$n(\mathbf{r}, t) = \sum_{i=1}^N |\psi_i(\mathbf{r}, t)|^2, \quad (4)$$

represented in terms of single-particle orbitals which in general have no physical meaning. As a result of TDDFT the many-electron TDSE can be exactly mapped onto a set of single-particle (time-dependent Kohn-Sham (TDKS)) equations, one for each electron

$$i\partial_t \psi_i(\mathbf{r}, t) = \hat{h}(t) \psi_i(\mathbf{r}, t), \quad i = 1, \dots, N, \quad (5)$$

where the TDKS hamiltonian is local and a unique functional of the exact density

$$\hat{h}(t) = -\frac{1}{2} \Delta + v_{ee}([n]; \mathbf{r}, t) + v_{\text{ext}}(\mathbf{r}, t) \quad (6)$$

$$v_{\text{ext}}(\mathbf{r}, t) = \frac{-Q_T}{r} + \frac{-Q_P}{|\mathbf{r} - \mathbf{R}(t)|}. \quad (7)$$

Even though the two hamiltonians (2) and (6) look similar there are a few remarkable differences. (i) While the many-electron hamiltonian is known, the explicit form of the TDKS hamiltonian is not. TDDFT only proves its existence. (ii) The electronic interaction  $\hat{V}_{ee}$  is time-independent, which is not the case for the single-particle counterpart:  $v_{ee}$  depends on time via the density, a feature we call response. This is the price to be paid for the simpler form of the TDKS equations (5).

To unfold various characteristics of the interelectronic potential one usually decomposes  $v_{ee}$  in different ways

$$v_{ee}([n]; \mathbf{r}, t) = v_H([n]; \mathbf{r}, t) + v_x([n]; \mathbf{r}, t) + v_c([n]; \mathbf{r}, t) \quad (8)$$

$$= v_{ee}([n_0]; \mathbf{r}) + \delta v_{ee}([n]; \mathbf{r}, t). \quad (9)$$

In equation (8)  $v_H$  denotes the Hartree potential which includes the classical screening effects due to the electronic charge distribution,  $v_x$  the exchange term due to the Pauli principle

and  $v_c$  the electronic correlation. In the following we will neglect the correlation term, thus approaching the TDKS equations from the time-dependent Hartree-Fock (TDHF) level. Equation (9) decomposes the interelectronic potential in terms of the stationary part of the undisturbed system prior to the collision and the response potential which is time-dependent due to the change of the electronic density during the collision. The gist of equations (8, 9) is to reveal different effects induced by the electronic interaction which can be observed in collision processes involving many active electrons.

## 2.2 The basis generator method

The numerical solution of the TDKS equations is a formidable task: not only does the competition between strong and weak channels impose a high accuracy demand in the time propagation of the density, but also the enormous delocalization of the ionization part of the electronic density has to be considered appropriately. Meanwhile one can find several strong methods in the literature which are able to meet these requirements: (i) lattice methods solving the TDSE in configuration <sup>5</sup>, or momentum <sup>6</sup> space, or a mixture thereof <sup>7</sup>, (ii) single-center <sup>8</sup> and two-center <sup>9</sup> expansion methods relying on different basis sets, (iii) the hidden crossing method <sup>10</sup> suitable for adiabatic impact energies, and (iv) different implementations of the classical trajectory Monte Carlo method <sup>11</sup> (for a review see e.g. <sup>12</sup>). We have developed our own tool, the basis generator method (BGM), which is essentially a time-dependent extension of the well known Krylow-space methods <sup>13</sup> for stationary systems. One starts with the definition of a generating basis, namely a finite set of eigenfunctions of the undisturbed system described by the hamiltonian  $\hat{h}_0$

$$\hat{h}(t) = \hat{h}_0 + \hat{v}_p(t) \quad (10)$$

$$\hat{h}_0|\phi_v^0\rangle = \varepsilon_v|\phi_v^0\rangle, \quad v = 1, \dots, V. \quad (11)$$

Then the hierarchy of pseudo-states defined by

$$\begin{aligned} |\phi_v^u\rangle &= (\hat{h} - i\partial_t)|\phi_v^{u-1}\rangle, \quad u = 1, \dots, U \\ &= (\hat{h} - i\partial_t)^u|\phi_v^0\rangle, \quad v = 1, \dots, V \end{aligned} \quad (12)$$

constitutes a finite model-space. As successive orders  $u$  are constructed by repeated application of the full Schrödinger operator  $\hat{h}(t) - i\partial_t$  the set of pseudo-states structurally follows the time propagation of the true quantum system <sup>14</sup>. In particular one can show that within a finite model-space only states of highest order  $U$  can interact with states of the infinite complementary space. I.e., if these states are not occupied during the time propagation, the exact solution of the TDSE stays in the model-space. Thus, the BGM provides a very general scheme and is valid for different hamiltonians.

The states defined in equation (12) become immediately very complicated

$$\begin{aligned} |\phi_v^1\rangle &= \hat{v}_p(t)|\phi_v^0\rangle \\ |\phi_v^2\rangle &= \left( -\frac{1}{2}\Delta\hat{v}_p(t) + \hat{v}_p(t)^2 - i\partial_t\hat{v}_p(t) - \nabla\hat{v}_p(t) \cdot \nabla \right) |\phi_v^0\rangle \end{aligned} \quad (13)$$

which is not surprising as the propagated wave function is complicated as well. However, one can show <sup>15</sup> that for hamiltonians (10) including only pure Coulomb potentials one finds a finite representation of the hierarchy (12) in terms of the states

$$|\chi_{\nu}^{\mu\mu'}\rangle = W_p^{\mu}W_t^{\mu'}|\phi_{\nu}^0\rangle, \quad \nu = 1, \dots, N(V), \quad \mu, \mu' = 1, \dots, M(U), \quad (14)$$

with  $W_{p/t}$  denoting the regularized Coulomb interaction with respect to the projectile and target center, respectively

$$\begin{aligned} W_t &= [x^2 + y^2 + z^2 + \epsilon^2]^{-\frac{1}{2}} \\ W_p &= [x_p^2 + y_p^2 + z_p^2 + \epsilon^2]^{-\frac{1}{2}} \end{aligned} \quad (15)$$

( $\epsilon$  can be interpreted as an arbitrarily small but finite 'nuclear radius'). In fact, this statement holds true also for potentials which can be represented in terms of an inverse power series of the distance like van der Waals potentials, etc.

For the results presented in chapter 3 we apply the simplified representation including only states generated with  $W_p$  which we believe to be reliable for positive charged ions colliding with atoms. For each Kohn-Sham orbital one, thus, makes the ansatz

$$\psi_j(\mathbf{r}, t) = \sum_{\mu=0}^{M(U)} \sum_{\nu=1}^{N(V)} c_{\mu\nu}^j(t) \chi_\nu^\mu(\mathbf{r}, t). \quad (16)$$

Inserting (16) into the TDKS equations (5) yields the set of coupled channel equations

$$i \sum_{\mu=0}^{M(U)} \sum_{\nu=1}^{N(V)} \dot{c}_{\mu\nu}^j(t) \langle \chi_\omega^\lambda | \chi_\nu^\mu \rangle = \sum_{\mu=0}^{M(U)} \sum_{\nu=1}^{N(V)} c_{\mu\nu}^j(t) \langle \chi_\omega^\lambda | \hat{h}(t) - i\partial_t | \chi_\nu^\mu \rangle. \quad (17)$$

### 2.3 Extraction of many-electron observables

The pivotal quantity of TDDFT is the single-particle density from which any many-electron observable can be derived in principle. This is however merely a mathematical statement and imposes a severe restriction on the theory, since most functionals for accessible observables are yet unknown. Within the non-correlation limit of TDDFT, however, the Kohn-Sham orbitals are assumed to carry the physical information about the active electrons and are therefore used to analyze the collision system at the independent particle model level. Within the orbital-picture one starts with the calculation of single-electron probability amplitudes for excitation and capture by projecting the  $N$  Kohn-Sham orbitals at some final collision time on target and travelling projectile states. As a consequence of the determinantal structure of the final wave function within the non-correlation picture, the inclusive probability  $P_{f_1, \dots, f_q}$  of finding  $q < N$  electrons in the states labeled  $f_1, \dots, f_q$ , while the remaining  $N - q$  electrons are not detected can be expressed as a  $q \times q$  determinant of the one-particle density matrix<sup>16</sup>

$$P_{f_1, \dots, f_q} = \det(\langle f_1 | \hat{n} | f_1 \rangle, \dots, \langle f_q | \hat{n} | f_q \rangle). \quad (18)$$

Higher inclusive probabilities, as for instance  $q$ -particle ionization  $P_q^{ion}$  or capture  $P_q^{cap}$  can then be deduced as ordered sums of the basic expression (18).<sup>17</sup>

In situations where the Pauli blocking in the final state is less important, the determinantal structure of inclusive probabilities breaks down to multinomial expressions of single-particle probabilities. If  $p_i^{exc}$ ,  $p_i^{cap}$  denote the sum over all excitation (including the elastic channel) and capture probabilities, respectively, total single-electron ionization and loss  $p_i^{ion}$ ,  $p_i^{loss}$  are deduced from unitarity

$$p_i^{ion} = 1 - p_i^{exc} - p_i^{cap} \quad (19)$$

$$p_i^{loss} = 1 - p_i^{exc} = p_i^{cap} + p_i^{ion}. \quad (20)$$

From these single-particle probabilities many-electron observables can be calculated. For instance, the net probabilities which indicate the average number of electrons lost, excited, captured or ionized during the collision are defined as the weighted sum over respective  $q$ -electron probabilities which again can be written as a sum over single-particle probabilities

$$P_{net}^x \equiv \sum_{q=1}^N q P_q^x = \sum_{q=1}^N p_q^x, \quad x: \text{ loss, cap, ion}. \quad (21)$$

Starting with the identity

$$\begin{aligned} 1 &= \prod_{i=1}^m (p_i^x + (1 - p_i^x))^{N_i} = \prod_{i=1}^m \sum_{q_i=0}^{N_i} \binom{N_i}{q_i} (p_i^x)^{q_i} (1 - p_i^x)^{N_i - q_i} \\ &= \sum_{q_1, \dots, q_m=0}^{N_1, \dots, N_m} \prod_{i=1}^m \binom{N_i}{q_i} (p_i^x)^{q_i} (1 - p_i^x)^{N_i - q_i} \end{aligned} \quad (22)$$

$q$ -particle probabilities for finding  $q$  electrons in channel  $x$  can be written as

$$P_q^x = \sum_{q_1, \dots, q_m=0, \sum_i q_i=q}^{N_1, \dots, N_m} \prod_{i=1}^m \binom{N_i}{q_i} (p_i^x)^{q_i} (1 - p_i^x)^{N_i - q_i}, \quad (23)$$

where  $m$  denotes the number of electron entities (e.g. electron shells) and  $N_i$  the number of electrons included in these entities. Obviously, the number of observables increases tremendously with the number of active electrons and it is impossible to cover all combinations of coincidences which might be of interest experimentally. Similarly to equation (23) one can calculate probabilities for  $k$ -fold capture associated with  $l$ -fold ionization  $P_{kl}$ . However, the straightforward multinomial analysis suffers from the problem that one obtains nonzero probabilities for unphysical higher-order capture events that correspond to the production of (multiply) negatively charged ions. In order to circumvent this flaw we introduced the analysis in terms of products of binomials<sup>18</sup>, in which the net electron capture  $P_{net}^{cap}$  is distributed over the physically allowed capture multiplicities  $k = 1, \dots, M$  by carrying out binomial statistics with a new single-particle probability  $P_{net}^{cap}/M$ .  $M$  is the number of electrons that can be accommodated by the projectile (typically smaller than the number of active electrons  $N$ ). The charge-state correlated probabilities  $P_{kl}$  are then obtained by multiplying the  $k$ -fold capture probabilities by independent  $l$ -fold binomial ionization probabilities (23)

$$P_{kl} = P_k^{cap} P_l^{ion}. \quad (24)$$

In cases, in which not only the target but also the projectile carries active electrons into the collision the statistical analysis has to be extended. The probabilities of interest  $P_{mn}$  for finding  $m$  electrons bound to the projectile and  $n$  electrons bound to the target after the collision are calculated by multiplying the  $P_{kl}$ 's for  $k$ -fold capture from the target to the projectile and  $l$ -fold target ionization with corresponding probabilities for capture and ionization of the active projectile electrons, and a subsequent summation of all contributing combinations.<sup>19</sup> Alternatively, the  $P_{mn}$  can be calculated via the inclusive probabilities (18), when the final wave function is assumed to be a single Slater determinant of *all* active (target and projectile) electrons. We will show in the next section that the Pauli blocking incorporated in this way may be crucial for the accurate calculation of specific processes in situations with active electrons on both centers.

### 3 Results

In this section we investigate the influence of different approximations in the effective potential (8, 9) on the propagation of the TDKS orbitals. The TDKS equations (5) are solved with the aid of the BGM pseudo-states defined in equation (16). The correlation term  $v_c([n]; \mathbf{r}, t)$  is neglected, approximating the TDKS equations by their exchange-only (i.e. Hartree-Fock (HF)) limit. Typical basis sets are constructed from a generating set of functions, representing the  $1s$  through  $4f$  orbitals of the HF ground state configuration of the target atom and a hierarchy of pseudo-states applying the operator  $W_p$  up to the order  $M = 8$  according to equation (14). From this basis we keep 120 states selected by a singular value decomposition of the overlap matrix. Each initially occupied orbital is propagated according to the coupled channel equations (17) assuming a straight line trajectory of the impacting projectile. The time propagation of active projectile electrons is carried out by an analogous BGM expansion in terms of undisturbed projectile states and a hierarchy of pseudo-states based upon the operator  $W_t$ . The scattered orbitals are analyzed at a final separation of  $45a_0$  and the many-electron observables are calculated from the multinomial expressions provided in section 2.3.

#### 3.1 Exchange effects

Exchange effects are investigated on the level of the exchange-only and no-response ( $\delta v_{ee}([n], \mathbf{r}, t) = 0$ ) approximations of equations (8, 9). Two functional forms of the exchange potential are compared: <sup>20</sup> (i) the homogeneous electron gas approximation with a long-range Latter correction of the self energy

$$v_x^{LDA}(n_0(\mathbf{r})) = \min\left\{-\frac{\alpha(3\pi^2 n_0(\mathbf{r}))^{1/3}}{\pi}, -\frac{1}{r}\right\}, \quad (25)$$

where for  $\alpha = 1$  one obtains the local density approximation (LDA), or for  $\alpha = 1.5$  the Hartree-Fock Slater (HFS) approximation and (ii) the optimized potential method <sup>21</sup> (OPM) yielding an integral equation for the local exchange term. The latter is known to be the best local approximation to the non-local HF exchange.

Figure 1 demonstrates clearly that the LDA exchange potential leads to wrong cross sections both at low and high energies in proton collisions with Ne and Ar atoms. In both regimes one overestimates the dominant electron removal process (capture and ionization respectively). The use of a correct local exchange potential (OPM) yields very accurate ionization cross sections and very reasonable capture results. As net electron loss is dominated by one-electron ionization or capture the agreement between the OPM results and the experimental data can be traced back to the fact that the first ionization potential depends crucially on the correct exchange potential <sup>22 20</sup>. Beside this global effect it has been found that the local behaviour of the exchange potential can introduce artificial structures in more differential observables like doubly differential cross sections for inclusive single-electron emission in  $\text{Au}^{53+}$ -Ar collisions. <sup>25</sup>

Now that we have demonstrated the role of static electronic exchange we turn to another quantum phenomenon associated with the fermionic nature of the atomic electrons. We consider the  $\text{He}^+(1s)$ -Ne collision system in which we demonstrate the role of overall antisymmetry for the  $(N + 1)$ -electron system. Two different analyses will be presented; they are both based on the same sets of single-particle orbital propagations (for  $\text{He}^+(1s)$ , as

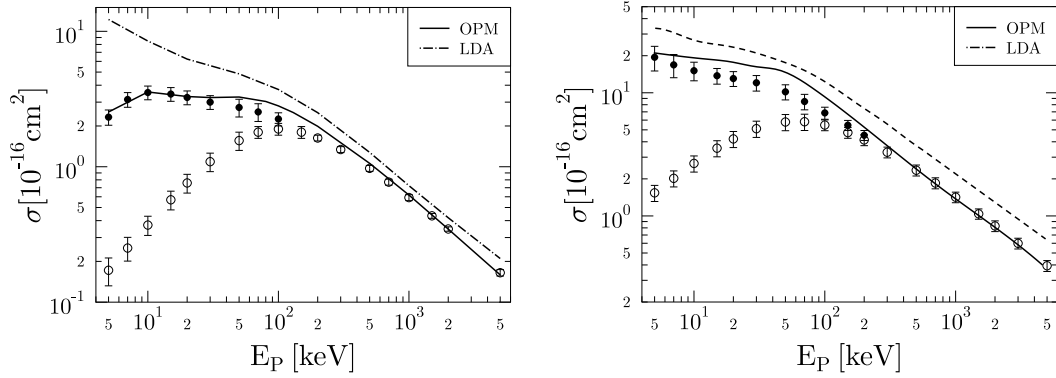


Figure 1. Net electron loss cross section (21) as a function of impact energy for p+Ne (left) and p+Ar (right).<sup>22</sup> Lines: BGM calculations with different exchange potentials; experimental data for (●) net electron loss<sup>23</sup> and (○) net ionization<sup>24</sup>.

well as the Ne(K,L) shells). In one case we compute probabilities based on equation (24) and form products of charge-state correlated probabilities that lead to specified electronic charge configurations on projectile and target. In the other case (termed Pauli) we form an  $(N + 1)$ -electron determinant from the propagated orbitals and perform the appropriate density matrix analysis.

Figure 2 shows an example of Pauli blocking that is easily explained: the calculation of neutralization of  $\text{He}^+(1s)$  by the 'products' analysis overestimates the result by almost a factor of 2, as both spin-up and spin-down orbitals are contributing and are not hindered by the fact that the dominant final  $\text{He}(1s^2)$  is a spin-singlet state. In a naive correction one would argue that only for one half of the Ne-orbitals the transfer is allowed, the rest would have to be distributed over other channels (perhaps the projectile continuum). The determinantal analysis which agrees rather well with experiment shows that the reduction is less than a factor of two due to some capture contributions into higher-lying orbitals of He.

Figure 3 shows an example of a more sophisticated Pauli correlation for which no obvious explanation is available. The channel of  $\text{He}^{2+}$  formation while summing over all final Ne-states can be described at high energies by a simple calculation with an active  $\text{He}^+$  electron and frozen target electrons (dotted curve). The remaining discrepancy with experiment at high energies can be explained as anti-screening.<sup>19</sup> At energies below 300 keV/amu the calculation overestimates the correct answer very badly, since it ignores the fact that at small impact parameters (for which  $\text{He}(1s)$  ionization occurs) a transfer of Ne-electrons to the projectile is very likely. The analysis in terms of products of probabilities corrects the situation (one multiplies the  $\text{He}^+$  ionization probability with the non-transfer probability for Ne(K,L)). Nevertheless, a discrepancy of almost a factor of 2 remains. The determinantal analysis corrects this situation: it re-distributes the transferred electron density from Ne(K,L) in such a way that the correct balance is obtained for  $\text{He}^0$ ,  $\text{He}^+$ , and  $\text{He}^{2+}$  formation. The latter cannot be obtained with a naive argument.

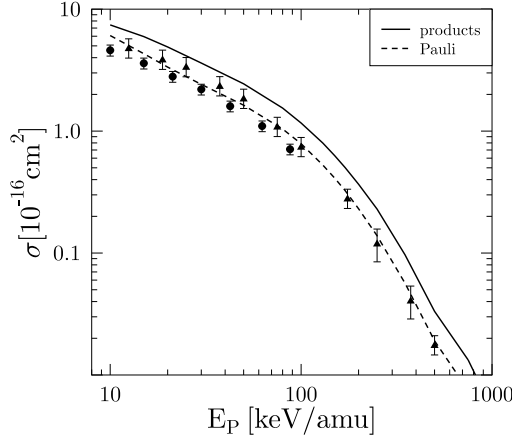


Figure 2. Total cross section for neutralization of the projectile as a function of impact energy for  $\text{He}^+ + \text{Ne}$  collisions. <sup>19</sup> Theory: BGM calculation with response and final-state analysis in terms of products of binomials (full curve) and inclusive analysis (broken curve). Experiment: circles <sup>26</sup>, triangles <sup>27</sup>.

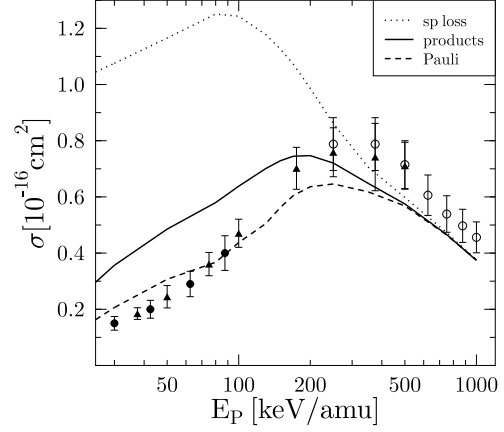


Figure 3. Total cross section for electron loss from the projectile as a function of impact energy for  $\text{He}^+ + \text{Ne}$  collisions. Theory: BGM calculation with response and final-state analysis in terms of products of binomials (full curve) and inclusive analysis (broken curve). The dotted curve corresponds to a single particle calculation for the active  $\text{He}^+$  electron. <sup>19</sup> Experiment: circles <sup>28</sup>, triangles <sup>27</sup>.

### 3.2 Response effects

In order to include time-dependent screening in the KS potential without increasing the computational effort considerably we introduced a simple model which accounts globally for charge-changing processes during the collision. <sup>29</sup> The effective target potential is approximated in terms of a linear combination of ionic potentials which yields an expression for the response potential that can be related to the undisturbed target potential with the time-dependence given by the  $q$ -fold electron loss probabilities as defined in equation (23)

$$\delta v_{ee}([n]; \mathbf{r}, t) \approx \frac{-1}{N-1} \sum_{q=1}^N (q-1) P_q^{loss}(t) v_{ee}([n_0]; \mathbf{r}) . \quad (26)$$

At which energies electronic response is of importance depends on the process considered. Two types of response have been incorporated in these calculations: dynamic target response was introduced <sup>29</sup> to make use of an effective single particle potential that depends on the electron removal probabilities from the target (23). It leads to a change in the multiple ionization cross sections at energies below 100 keV/amu for  $q = 1$ , and at energies below 1 MeV/amu for  $q = 5$  in  $\text{C}^{4+} + \text{Ne}$  collisions (Figure 5). <sup>30</sup>

Projectile response is a more subtle phenomenon. In analogy to the dynamic response at the target one introduces a screening on the projectile which depends on the amount of probability in bound projectile states. The propagated orbitals can be projected onto moving projectile eigenstates as a function of time. For technical reasons (computational economy) this information is obtained after the computation of the time evolution. Figure 4 demonstrates for the case of the net capture probability in  $b=1.75$  a.u.  $\text{C}^{4+} - \text{Ne}$  collisions at



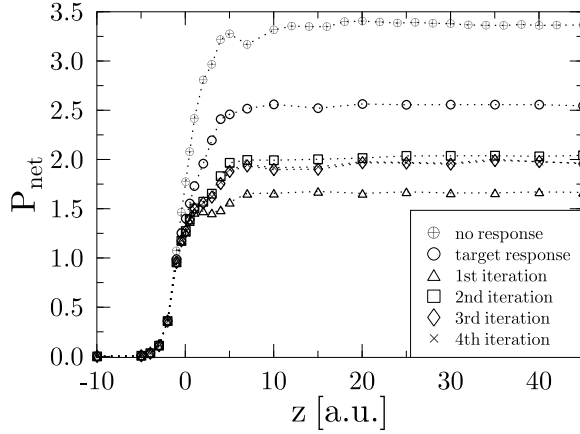


Figure 4. Net electron capture probability according to equation (21) as a function of the scaled time  $z = v_P t$  at  $E_P=20$  keV/amu and  $b=1.75$  a.u. in  $C^{4+} + Ne$  collisions.

20 keV/amu how an iterative approach converges for the entire time evolution. Of physical relevance is the comparison of asymptotic values (transfer on average of 3.35, 2.55, and 2.0 electrons respectively in the 'no-response', 'target response', and 'target-and-projectile response' models).

In Figure 5 we demonstrate for  $C^{4+}$ -Ne calculations that the overall effect of projectile

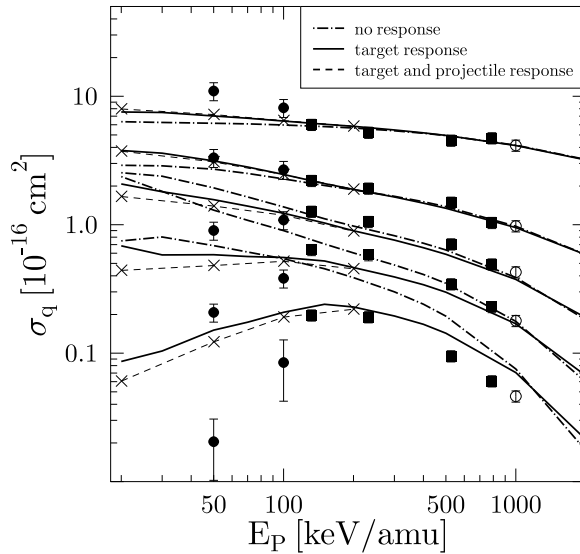


Figure 5. Total cross sections for  $q$ -fold electron loss as a function of impact energy. Theory: BGM calculations for  $C^{4+} + Ne$  collisions in the no-response (chain curve), target response (full line), and target-and-projectile response (dashed line) approximation, respectively. Experiment:  $C^{4+}$  projectiles; ( $\bullet$ )  $^{31}$ ; full squares  $^{32}$ , ( $\circ$ )  $^{33}$ .

response on charge-state correlated cross sections is significant only for those channels that are dominated by small impact parameters. The effect is largest at the smallest energies, but our calculations are not extended below 20 keV/amu, as one might be leaving the validity regime of the no-correlation approach of the TDKS equations, and adiabatic correlations might begin to dominate the physical channels.

### 3.3 Effective scaling in the net electron loss cross section

Finally, we would like to draw attention to a surprising result obtained within the 'target response' approximation, and which appears not to be altered by adding projectile response. In Figure 6 we show a rather global quantity, namely the scaled net electron removal cross section for  $X^{Q_P+}$  ions colliding with Ne atoms over a broad range of reduced energies  $E_P/Q_P$ . The experimental data comprise a variety of results which include bare and non-bare ions, and which were compared to our results for  $Q_P = 2$  and  $Q_P = 4$  before.<sup>30</sup> In Figure 6 we have included new calculations for  $Q_P = 3, 5, 6, 8$ . It is remarkable that

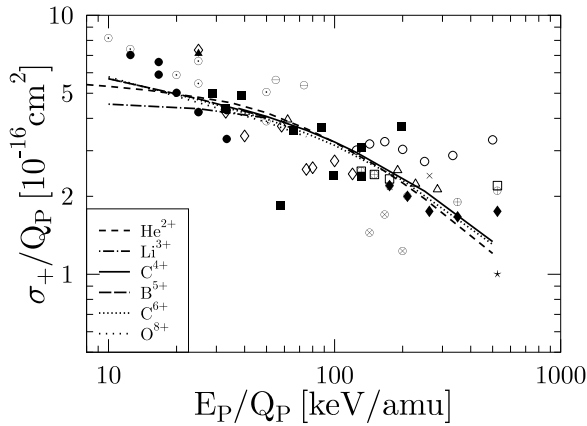


Figure 6. Total cross section for net recoil ion production divided by the projectile charge as a function of the impact energy divided by the projectile charge for Ne targets. Theory: BGM-calculations in the target-response approximation. The sources of the experimental data are listed in<sup>30</sup>.

the 'target response' approximation yields an almost universal curve for the scaled cross section over a considerable range of energies. The 'no response' approximation does not follow this scaling behaviour, and the  $Q_P = 1$  results in particular (not included in Fig. 6) are consistently below the approximately universal result<sup>30</sup>. At large values of  $E_P/Q_P$  we notice some deviations from scaling due to the  $\ln(cE_P)/E_P$  dependence of our quantum mechanical calculations. In this sense the present result is quite different from the previously obtained scaling behaviour in the CTMC-IPM work of Olson<sup>7</sup>. The present cross section is lower at all energies than the classical trajectory result which appears to follow  $Q_P^2/E_P$  scaling up to very high energies. We note that the latter result was actually obtained at higher energies and higher projectile charges as compared to the included experiments, as well as the present calculations.

At the left-hand side of the graph, i.e., for moderate values of  $E_P/Q_P$  the scaling is unexpected, since the actual probabilities as a function of impact parameter show a rather different behaviour, and it is only the area under the curve  $bP_{\text{net}}(b)$  which is approximately universal. We also note that for different values of  $Q_P$  at the same value of  $E_P/Q_P$  the process by which electrons are removed from the target varies: capture and ionization compete with each other in this energy regime.

At present the experiments are not sufficiently accurate to prove or disprove the proposed scaling behaviour. In fact, the absolute uncertainty in most results is so large (of order 50%) that one cannot infer an accurate energy dependence from the experimental data<sup>30</sup>. We suggest that new experiments be carried out with a sufficiently accurate absolute normalization to test the prediction made by the present model calculations.

## 4 Conclusion

The results of the previous section exhibit very different facets of the electronic interaction in a dynamical quantum system. We have studied in some detail exchange and response effects which are usually embraced by the term *electronic screening*.

It is important to understand that the appearance of effects due to the inter-electronic potential depends on the particular observable of the collision system. Exchange effects, for instance, are important for total electron removal processes and largely dominate response effects, whereas the latter are crucial for a quantitative understanding of  $q$ -particle loss processes in the same collision system. Pauli-blocking on the other side strongly depends on the density of states of open final channels: while multiple ionization is well described in terms of products of single-particle probabilities, capture into low lying states of the projectile needs a careful determinantal analysis of the final wave function.

With this experience it is crucial to avoid intuitive modeling of the effective electronic potential in favour of a rigorous a priori approximation of the many-electron hamiltonian in order to obtain a deeper understanding of the different phenomena which can be observed in many-electron collisional systems.

## Acknowledgments

This work has been supported partly by Collaborative Research Grant No. 972997 of the NATO International Scientific Exchange Program and by the Natural Sciences and Engineering Research Council of Canada. One of us (T.K.) gratefully acknowledges the financial support of the DAAD.

## References

1. J. Ullrich, R. Moshhammer, R. Dörner, O. Jagutzki, V. Mergel, H. Schmidt-Böcking, and L. Spielberger, J. Phys. B **30**, 2917 (1997);  
R. Dörner, V. Mergel, O. Jagutzki, L. Spielberger, J. Ullrich, R. Moshhammer, and H. Schmidt-Böcking, Phys. Rep. **330**, 95 (2000).
2. R. Nagano, K. Yabana, T. Tazawa, and Y. Abe, J. Phys. B **32**, L65 (1999);  
R. Nagano, K. Yabana, T. Tazawa, and Y. Abe, Phys. Rev. A **62**, 062721 (2000).
3. J.M. Rost and J.S. Briggs, Eur. Phys. J. D **10**, 311 (2000).
4. E.K.U. Gross, J.F. Dobson, and M. Petersilka in Topics in Current Chemistry 181, ed. R.F. Nalewajski (Springer, Heidelberg, 1996).
5. M. Horbatsch in Proc. 14th Int. Conf. on the Application of Accelerators in Research and Industry, Denton, AIP Conf. Proc. **392**, 71 (1997);  
D.R. Schultz, M.R. Strayer, and J.C. Wells, Phys. Rev. Lett. **82**, 3976 (1999).
6. D.C. Ionescu and A. Belkacem, Physica Scripta **T80**, 128 (1999).
7. M. Chassid and M. Horbatsch, J. Phys. B **31**, 515 (1998);  
A. Kolakowska, M. Pindzola, F. Robicheaux, D.R. Schultz, and J.C. Wells, Phys. Rev. A **58**, 2872 (1998);  
A. Kolakowska, M. Pindzola, and D.R. Schultz, Phys. Rev. A **59**, 3588 (1999).
8. B. Pons, Phys. Rev. A **63**, 012704 (2001); *ibid* **64**, 019904 (2001);  
K. Sakimoto, J. Phys. B **33**, 5165 (2000);

- A. Igarashi, S. Nakazaki, and A. Ohsaki, Phys. Rev. A **61**, 062712 (2000);  
X.M. Tong, D. Kato, T. Watanabe, and S. Ohtani, Phys. Rev. A **62**, 052701 (2000).
9. J. Fu, M.J. Fitzpatrick, J.F. Reading, and R. Gayet, J. Phys. B **34**, 15 (2001);  
E.Y. Sidky, C. Illescas, and C.D. Lin, Phys. Rev. Lett. **85**, 1634 (2000);  
N. Toshima, Phys. Rev. A **59**, 1981 (1999).
  10. E.A. Solov'ev, Sov. Phys. Usp. **32**, 228 (1989);  
M. Pieksma and S.Y. Ovchinnikov, J. Phys. B **27**, 4573 (1994).
  11. C.L. Cocke and R.E. Olson, Phys. Rep. **205**, 163 (1991);  
M. Horbatsch, Phys. Rev. A **49**, 4556 (1994);  
C. Illescas and A. Riera, Phys. Rev. A **60**, 4546 (1999).
  12. T. Kirchner, H.J. Lüdde, O.J. Kroneisen, and R.M. Dreizler, Nucl. Instr. and Meth. B **154**, 46 (1999).
  13. R. Kosloff, Ann. Rev. Phys. Chem. **45**, 145 (1994).
  14. H.J. Lüdde, A. Henne, T. Kirchner, and R.M. Dreizler, J. Phys. B **29**, 4423 (1996).
  15. O.J. Kroneisen, H.J. Lüdde, T. Kirchner, and R.M. Dreizler, J. Phys. A **32**, 2141 (99).
  16. H.J. Lüdde and R.M. Dreizler, J. Phys. B **16**, 3973 (1983);  
H.J. Lüdde and R.M. Dreizler, J. Phys. B **18**, 107 (1985).
  17. P. Kürpick, H.J. Lüdde, W.D. Sepp, and B. Fricke, Z. Phys. D **25**, 17 (1992);  
H.J. Lüdde, A. Macias, F. Martin, A. Riera, and J.L. Sanz, J. Phys. B **28**, 4101 (1995).
  18. T. Kirchner, H.J. Lüdde, M. Horbatsch, and R.M. Dreizler, Phys. Rev. A **61**, 052710 (2000).
  19. T. Kirchner and M. Horbatsch, Phys. Rev. A **63**, 062718 (2001).
  20. T. Kirchner, L. Gulyas, H.J. Lüdde, E. Engel, and R.M. Dreizler, Phys. Rev. A **58**, 2063 (1998).
  21. J.D. Talman and W.F. Shadwick, Phys. Rev. A **14**, 36 (1976);  
E. Engel and S.H. Vosko, Phys. Rev. A **47**, 2800 (1993).
  22. T. Kirchner, L. Gulyas, H.J. Lüdde, A. Henne, E. Engel, and R.M. Dreizler, Phys. Rev. Lett. **79**, 1658 (1997).
  23. M.E. Rudd, R.D. DuBois, L.H. Toburen, C.A. Ratcliffe, and T.V. Goffe, Phys. Rev. A **28**, 3244 (1983).
  24. M.E. Rudd, Y.K. Kim, D.H. Madison, and J.W. Gallagher, Rev. Mod. Phys. **57**, 965 (1985).
  25. L. Gulyas, T. Kirchner, T. Shirai, and M. Horbatsch, Phys. Rev. A **62**, 022702 (2000).
  26. M.E. Rudd, T.V. Goffe, A. Itoh, and R.D. DuBois, Phys. Rev. A **32**, 829 (1985).
  27. R.D. DuBois, Phys. Rev. A **39**, 4440 (1989).
  28. M.M. Sant'Anna, W.S. Melo, A.C.F. Santos, G.M. Sigaud, and E.C. Montenegro, Nucl. Inst. and Meth. B **99**, 46 (1995).
  29. T. Kirchner, M. Horbatsch, H.J. Lüdde, and R.M. Dreizler, Phys. Rev. A **62**, 042704 (2000).
  30. T. Kirchner, M. Horbatsch, and H.J. Lüdde, Phys. Rev. A **64**, 012711 (2001).
  31. Y. Sugizaki, M. Sataka, K. Kawatsura, T. Shirai, and Y. Nakai, J. Phys. B **22**, 263 (1989).
  32. S. Kelbch *et al.*, J. Phys. B **23**, 1277 (1990).
  33. O. Heber *et al.*, Phys. Rev. A **52**, 4578 (1995).
  34. A.S. Schlachter, K.H. Berkner, W.G. Graham, R.V. Pyle, P.J. Schneider, K.R. Stalder, J.W. Stearns, J.A. Tanis, and R.E. Olson, Phys. Rev. A **23**, 2331 (1981).